# Energy & Environmental Science

## Accepted Manuscript

This article can be cited before page numbers have been issued, to do this please use: L. Liao, S. Wang, J. Xiao, X. Bian, Y. Zhang, M. D. Scanlon, X. Hu, Y. Tang, H. H. Girault and B. Liu, *Energy Environ. Sci.*, 2013, DOI: 10.1039/C3EE42441C.

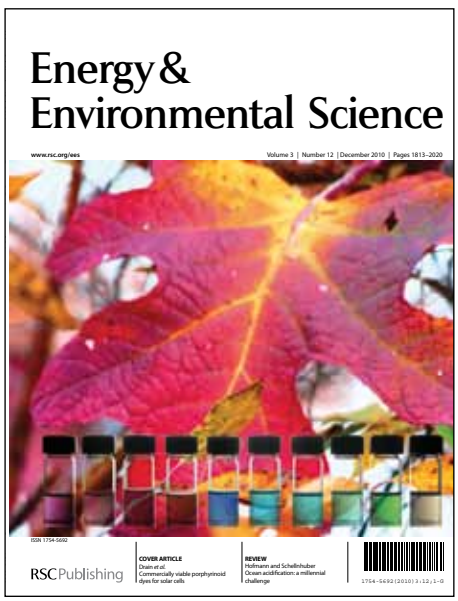


This is an *Accepted Manuscript*, which has been through the RSC Publishing peer review process and has been accepted for publication.

*Accepted Manuscripts* are published online shortly after acceptance, which is prior to technical editing, formatting and proof reading. This free service from RSC Publishing allows authors to make their results available to the community, in citable form, before publication of the edited article. This *Accepted Manuscript* will be replaced by the edited and formatted *Advance Article* as soon as this is available.

To cite this manuscript please use its permanent Digital Object Identifier (DOI®), which is identical for all formats of publication.

More information about *Accepted Manuscripts* can be found in the **Information for Authors**.

Please note that technical editing may introduce minor changes to the text and/or graphics contained in the manuscript submitted by the author(s) which may alter content, and that the standard **Terms & Conditions** and the **ethical guidelines** that apply to the journal are still applicable. In no event shall the RSC be held responsible for any errors or omissions in these *Accepted Manuscript* manuscripts or any consequences arising from the use of any information contained in them.

View Article Online
DOI: 10.1039/C3EE42441C



## Table of Contents

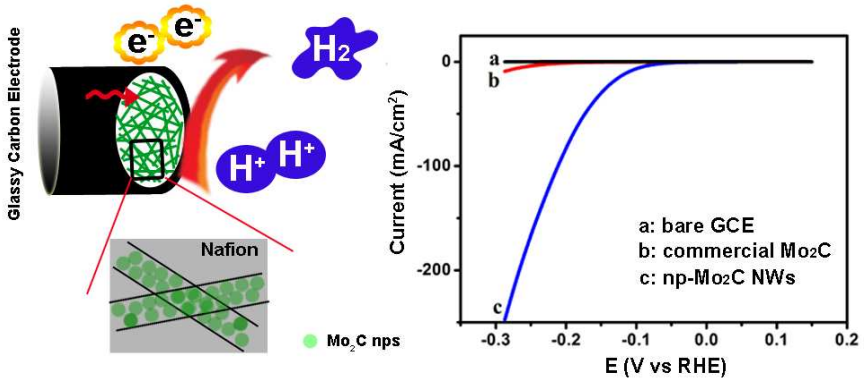


Nanoporous molybdenum carbide nanowires exhibit superior electrocatalytic activity towards hydrogen evolution reaction attributed to abundant nanoporosity, large surface area and high dispersibility of np-$Mo_2C$ NWs.

View Article Online
DOI: 10.1039/C3EE42441C

# Nanoporous Molybdenum Carbide Nanowire as an Electrocatalyst for the Hydrogen Evolution Reaction

Lei Liao,[a+] Sinong Wang,[a+] Jingjing Xiao,[a] Xiaojun Bian,[a] Yahong Zhang,[a] Michael D. Scanlon,[b] Xile Hu,[c] Yi Tang,[a*] Baohong Liu,[a*] and Hubert H. Girault[b]

[a]Department of Chemistry, State Key Lab of Molecular Engineering of Polymers and Laboratory of Molecular Catalysis and Innovative Materials, Fudan University, Shanghai 200433, P. R. China; *Email: bhliu@fudan.edu.cn, yitang@fudan.edu.cn;

[+]The authors contributed equally to this work.

[b]Laboratoire d'Electrochimie Physique et Analytique, Ecole Polytechnique Fédérale de Lausanne, CH-1015 Lausanne, Switzerland; Email: Hubert.Girault@epfl.ch;

[c]Laboratory of Inorganic Synthesis and Catalysis, Ecole Polytechnique Fédérale de Lausanne, CH-1015 Lausanne, Switzerland.

**Abstract**

A highly active and stable electrochemical catalyst of nanoporous molybdenum carbide nanowires (np-$Mo_2C$ NWs) has been developed for the hydrogen evolution reaction (HER). The np-$Mo_2C$ NWs were synthesized simply by pyrolysis of a $MoO_X$/amine hybrid precursor with sub-nanosized periodic structure under an inert atmosphere. The enriched nanoporosity and large reactive surface of these highly dispersed nanowires with uniform $Mo_2C$ nanocrystallites provides an efficient electrocatalysis, leading to their superior HER activity with lower onset overpotential and higher current densities

View Article Online
DOI: 10.1039/C3EE42441C

than $Mo_2C$ microparticles. This study opens a new perspective for the development of highly active non-noble electrocatalysts for hydrogen production from water splitting.

**Keywords:** Molybdenum Carbide; hydrogen evolution; water splitting; electrocatalysis; electrochemistry; energy.

## Introduction

Sustainable hydrogen production from water splitting is one of the most attractive methods for energy storage and conversion.[1-4] Electrolysis of water has been studied for several decades, but both the hydrogen evolution reaction (HER) and the oxygen evolution reaction (OER) still remain technical challenges. Although platinum (Pt)-based materials have proved to be the most effective HER electrocatalysts, their high cost and low abundance limits their large-scale applications.[5-9] Therefore, some Pt-like materials with cheap and abundant elements have attracted considerable attention as alternative catalysts or catalyst supports for various applications, which sometimes even offer significant advantages over noble metals.[10-14] Among these, transition metal carbides display remarkable catalytic activities, owing to their similar electronic and catalytic properties to Pt-group metals (by inducing carbon into the metal lattice), and have been identified as the most promising candidates to replace or reduce Pt employment in catalysis reactions.[15-18] Additionally, they have been used as stable supports for precious metals over different ranges of pH.[19] Recently, Vrubel and Hu reported that after removal of surface oxides, the commercial molybdenum carbide

View Article Online
DOI: 10.1039/C3EE42441C



($Mo_2C$) was a very active HER catalyst in both acidic and basic conditions.[20] However, the use of aggregated $Mo_2C$ microparticles may hamper the transport of electrons or protons during the reaction, and thereby result in a loss of activity, given that the performance of HER electrocatalysts greatly depends on their compositions and structures.[20] Recently, Sasaki *et al.* demonstrated that $Mo_2C$ nanoparticles on carbon nanotubes were indeed a highly active and durable electrocatalyst for hydrogen production.[21] In the present paper, we have developed nanopore-structured $Mo_2C$ nanowires to increase the specific surface area for reaction. These nanowires are composed of individual nanocrystallites, each of which are closely interconnected to shorten the electron transfer pathway but free of large aggregation. It is anticipated that such nanowire catalysts with abundant porosity not only possess more exposed active surface but also enable the rapid diffusion of ions and electrons favoring a better activity.

The purpose of this work is to demonstrate the prominent HER performance of nanoporous $Mo_2C$ nanowires composed of $Mo_2C$ nanocrystallites (np-$Mo_2C$ NWs). The np-$Mo_2C$ NWs were prepared by a strategy developed in our group through simply pyrolyzing precursor MoOx/amine hybrid nanowires under an inert atmosphere.[22, 23] The sub-nanometer contact between molybdenum oxides and amine molecules in the precursor creates a quasi-homogenous reaction environment and greatly facilitates the formation of the nanocrystallite-composed nanoporous structure.[21] The special features of large active surface areas, nanosized crystallites and enriched nanoporosity of np-$Mo_2C$ NWs greatly accelerates their interfacial electrocatalytic reactions while

View Article Online
DOI: 10.1039/C3EE42441C



allowing rapid charge transfer kinetics. As a result, superior electrocatalytic activity towards hydrogen production is seen compared with bulk $Mo_2C$ particles and other nonprecious metal materials. Using electrochemical impedance spectroscopy, the very high current densities at np-$Mo_2C$ NWs-modified electrode are attributed to the considerable increase of electrochemically active surface area as well as the smaller charge-transfer resistances and higher interfacial capacitances.

## Results and discussion

### Characterization of np-$Mo_2C$ NWs

Figure 1 presents the typical morphology, structure, composition and porosity of the np-$Mo_2C$ NWs sample, which were prepared by calcination of the organic-inorganic hybrid $Mo_3O_{10}(C_6H_8N)_2 \cdot 2H_2O$ nanowire precursor at 725 $^oC$ in an inert flow.[22] The scanning electron microscopy (SEM) image clearly revealed the uniform 1D morphology of each individual np-$Mo_2C$ NW being several micrometers in length and 80-150 nm in width (Figure 1A). Furthermore, high-resolution transmission electron microscopy (HRTEM) showed that such nanowires were composed of nanocrystallites of about 10-15 nm in size (Figure 1B and 1C), significantly differing from the morphology of larger and more irregular bulk commercial $Mo_2C$ particles (Figure S1).[20] Elemental analysis by energy dispersive spectroscopy (EDS) confirmed that the Mo and C contents were consistent with their theoretical values in $Mo_2C$ (Figure 1D), while X-ray diffraction (XRD) confirmed the hexagonal phase structure of the $Mo_2C$ nanowires (Figure 1E). Meanwhile, the results calculated from the $N_2$ sorption isotherm

View Article Online
DOI: 10.1039/C3EE42441C



(Figure 1F) show a BET surface area of 63.9 $m^2/g$ and a mesopore size of 3.3 nm resulting from the aggregation of $Mo_2C$ nanocrystallites inside the nanowires. Thus, taking into account the evidence from each characterization technique, we can summarize that the np-$Mo_2C$ NWs possess uniform one-dimensional morphology, nanosized crystallites, enriched nanoporosity and large surface areas. Such a combination of beneficial attributes would significantly enhance the catalytic potency of np-$Mo_2C$ NWs towards the HER by not only providing abundant specific catalytic sites but also facilitating the access of electrolytes and allowing rapid charge transfer kinetics. For comparison with both commercial $Mo_2C$ and np-$Mo_2C$ NWs, we synthesized nanoporous $Mo_2C$ flakes composed of nanocrystallites about 20-25 nm in size and bulky $Mo_2C$ foams composed of large particles. Their respective SEM and TEM images, as well as XRD patterns, are presented in Figures S2-S4. The porosity of the $Mo_2C$ flakes and bulky $Mo_2C$ foams resulted from the aggregation of crystallites inside the $Mo_2C$. Nitrogen adsorption/desorption isotherms (Figure S5) show BET surface areas of 67.6 $m^2/g$ and 30.3 $m^2/g$, average pore sizes of 4.5 nm and 3.7 nm, and pore volumes of 0.09 $cm^3/g$ and 0.04 $cm^3/g$ for the $Mo_2C$ flakes and bulky foams, respectively.

**HER catalytic activities of np-$Mo_2C$ NWs modified electrodes**

The electrocatalytic HER activity of the np-$Mo_2C$ NWs sample was investigated by depositing them on a glassy carbon electrode (GCE) with a catalyst loading of 0.21 $mg/cm^2$ (np-$Mo_2C$ NW-modified GCE). The experiment is conducted in 0.5 M $H_2SO_4$ solution at room temperature using a three-electrode setup. For comparison, GCEs were

View Article Online
DOI: 10.1039/C3EE42441C





also modified with commercial $Mo_2C$ particles (comm-$Mo_2C$-modified GCE), nanoporous $Mo_2C$ flakes (flaky $Mo_2C$-modified GCE), bulky $Mo_2C$ foams (bulky $Mo_2C$-modified GCE) as well as a physical mixture of np-$Mo_2C$ NWs and Vulcan carbon (np-$Mo_2C$ NW/carbon-modified GCE). Figure 2A shows the polarization curves (*i*-*V* plot) recorded for each individual electrode. For a np-$Mo_2C$ NW-modified GCE, the catalytic current was observed at a low onset overpotential of about 70 mV (*vs* RHE). This current is ascribed to the HER, rather than other processes, due to the similarity of impedance at various HER overpotentials from 70 to 150 mV (Figure 3). Beyond this, the cathodic current rises rapidly at more negative potentials with substantial current densities of ca. 60 mA/cm$^2$ at an overpotential of 200 mV. Such electrocatalytic activity is one of the best reported for non-noble catalysts in acidic media to-date. In contrast, a comm-$Mo_2C$-modified GCE showed much less HER activity, with current densities of only 1.2 mA/cm$^2$ at 200 mV (Figure 2A), less than 1/50 of those at the np-$Mo_2C$ NW-modified GCE. Similarly, a synthesized bulky $Mo_2C$-modified GCE also showed a low current density of 7.3 mA/cm$^2$ at 200 mV (Figure S6). Both commercial and bulky $Mo_2C$ particles had smaller surface areas and exhibited lower catalytic activities, indicating that surface area is a crucial structural parameter dominating the HER, as reported widely in the literatures. However, the catalytic current density derived from the synthesized nanoporous bulky $Mo_2C$ was about 6 times higher than that of the comm-$Mo_2C$-modified GCE. The existence of porosity can prevent the large aggregation between crystallites endowing them with more exposed active surface and also enabling the rapid diffusion of species during the

View Article Online
DOI: 10.1039/C3EE42441C



reactions. On the other hand, the flaky $Mo_2C$-modified GCE gave a current density of 21 mA/cm$^2$ at 200 mV (Figure S6), higher than that of bulky $Mo_2C$ particles while a little lower than that of a np-$Mo_2C$ NW-modified GCE. The results showed that crystallite size was another factor influencing the HER catalysis consistent with the results reported by Sasaki.[21] As discussed above, the significantly improved catalytic activity of a np-$Mo_2C$ NWs-modified GCE derives from a potent combination of specific structural properties, namely large surface areas, high dispersibility, nanosized crystallites and abundant nanoporosity, contributing in turn to the high abundance of available catalytic active sites, less particle aggregation and smaller charge-transfer resistances of the electrode.

To illustrate the relative enhancement of catalytic activity for np-$Mo_2C$ NWs, electrochemical impedance spectroscopy (EIS) was further applied at various HER overpotentials for this system. The Nyquist and Bode plots of the EIS response are shown in Figure 3. The np-$Mo_2C$ NW-modified electrode exhibited two semicircles at all applied potentials, indicating that the corresponding equivalent circuit for the HER was characterized by two time constants as fitted from the experimental data (Figure S8). The first one at high frequencies is related to the porous property of the electrode's surface; whereas another with potential-dependent properties at low frequencies is attributed to the kinetics of the HER process.[24-26] Bode plots also display two relaxation times where the high-frequency relaxation time is constant at these overpotentials. The similar impedance properties observed indicated similar electrochemical processes with regard to the HER at all of these overpotentials. Indeed, catalytic currents and hydrogen

View Article Online
DOI: 10.1039/C3EE42441C



bubbles were clearly observed at a potential of 70 mV. Such superior electrocatalytic activity of np-$Mo_2C$ NWs towards the HER was also validated by observation of lower charge-transfer resistance and higher interfacial capacitances derived from the second semicircles (associated with fast reaction kinetics and considerable increases of the electrochemically accessible surface area after nanowire modification). Figure S9 presents the low-frequency charge transfer resistance ($R_{ct}$) and constant phase element (CPE) as a function of the HER overpotentials. The recorded values of $R_{ct}$ decrease from 780 Ω at 80 mV to 90 Ω at 150 mV. Application of more negative potentials decreases the double-layer capacitance, from ~9.5 mF/cm$^2$ (45.2 mF/mg) at 80 mV to ~4.3 mF/cm$^2$ (20.5 mF/mg) at 150 mV, probably due to partial blocking of the electrode surface sites by freshly generated hydrogen species. At more negative potentials, hydrogen bubble evolution is more vigorous at the electrode surface. The high values of double-layer capacitance for the nanoporous np-$Mo_2C$ NW-modified electrodes further illustrate their porous character due to being composed of nanosized crystallites with large specific surface areas.[27,28] Both lower charge-transfer resistance and higher interfacial capacitance demonstrate the superior electrocatalytic activity of np-$Mo_2C$ NWs.

The Tafel slope of the amperometric response for a catalyst-modified electrode is an inherent property indicative of the rate-limiting step for the HER. Tafel analysis allows a distinction of the possible mechanistic steps occurring during the HER at an electrode surface. In acidic solution, three separate reaction steps are possible when hydrogen is evolved at the catalyst modified electrode surface.

View Article Online
DOI: 10.1039/C3EE42441C



Discharge reaction: $H_3O^+ + e^- + cat \rightarrow cat\text{-}H + H_2O$ (Volmer-reaction)

Combination reaction: $cat\text{-}H + cat\text{-}H \rightarrow 2cat + H_2$ (Tafel-reaction)

Ion + atom reaction: $H_3O^+ + e^- + cat\text{-}H \rightarrow cat + H_2 + H_2O$ (Heyrovsky-reaction)

According to previous reports, a Tafel slope of 30 mV/decade suggests the mechanism proceeds through the Volmer-Tafel mechanism and the recombination step is rate-limiting.[29] A Tafel slope of 40 mV/decade suggests hydrogen production *via* the Volmer-Heyrovsky mechanism and the electrochemical desorption step is rate-limiting.[30] Finally, a Tafel slope of 120 mV/decade may arise from various reaction pathways depending on the surface coverage of adsorbed hydrogen.[29] The linear portions of the Tafel plots are fitted to the Tafel equation ($\eta = b \log j + a$, where $j$ is the current density and b is the Tafel slope), yielding Tafel slopes of ~53 mV/decade ($\eta$ = 80-100 mV) and ~78 mV/decade ($\eta$ = 180-200 mV) for np-$Mo_2C$ NWs and commercial $Mo_2C$, respectively (Figure 2B). Obtaining a Tafel slope, however, is subjective with moderately different values possible by judicious choice of the regions on the current voltage curves to analyse. Additional complications may arise from the different ways in which the *iR*-drops are corrected. With this in mind, the Tafel slopes of ~53 and ~78 mV/decade for np-$Mo_2C$ NWs and commercial $Mo_2C$, respectively, are somewhat ambiguous with regard to elucidating the precise HER mechanism at each catalyst modified GCE. One possible conclusion is to eliminate the Volmer-step as the rate determining step, but beyond that only speculation is possible without the intervention of more powerful mechanistic analysis tools. Therefore, the clear perspective now that np-$Mo_2C$ NWs have been identified as highly active catalysts is to develop a new suite

View Article Online
DOI: 10.1039/C3EE42441C



of techniques that go beyond a routine Tafel analysis based on polarisation curves. Although electron transport (ET) is integral to the HER mechanism, precise analysis of ET at a catalyst modified GCE can be masked by the multiple proton-coupled electron transfer reactions occurring during a typical HER process. To circumvent this issue, recently, Vrubel *et al.* highlighted the benefits of transitioning from linear sweep voltammetry (LSV)-based analysis to electrochemical impedance spectroscopy (EIS)-based analysis of Tafel slopes.[31] They demonstrated the possibility of identifying a slow electron transport process in the HER catalysed by molybdenum sulfides. This method is directly beneficial to the analysis of $Mo_2C$-based electrocatalysts as it is amenable to the study of catalysts of poor electronic conductivity. The latter is a dominant catalyst attribute that may limit the scalability of a catalysts use (*i.e.* increased resistance to ET in thicker catalyst films) and, additionally, an EIS-based approach should provide less subjective data on the improvements of a catalysts activity by decreases in ET resistance on either physical mixing of the catalyst with carbon materials or direct immobilisation of the catalyst on a carbon support, as discussed *vida infra*. A plot of log $Rct^{-1}$ *vs.* overpotential (Figure S10) gives a Tafel slope ~60 mV/decade ($\eta$ = 70-100 mV) for np-$Mo_2C$ NWs from the EIS data. A Tafel slope obtained in this way reflects purely the charge transfer kinetics, in contrast to a Tafel slopes obtained from voltammetry data which may include contributions from catalyst resistance.[31] Although the Tafel slopes obtained by both methods are comparable, such values do not allow a clear distinction between which of the Heyrovsky or Tafel reactions are rate-limiting, and further mechanistic studies are required in this direction.

View Article Online
DOI: 10.1039/C3EE42441C



Stability of the catalytic response is evaluated by cycling the np-$Mo_2C$ NW-modified GCE continuously for 1000 cycles. At the end of the cycling procedure, the catalyst affords similar *i-V* curves to the initial cycle with negligible loss of the cathodic current (Figure 4). The long-term stability of np-$Mo_2C$ NWs was also tested by electrolysis at a fixed potential. Figure 4, inset, shows that the catalytic currents remain around at ca. 12 mA/cm$^2$ over 25 hours demonstrating that np-$Mo_2C$ NWs are stable catalysts under the experimental conditions employed for this catalysis system.

Moreover, when np-$Mo_2C$ NWs were physically mixed with commercial Vulcan carbon (1:1 w/w) and used to modify GCEs, an enhanced catalytic performance was observed to that of a pure np-$Mo_2C$ NW-modified GCE (Figure 5A) with substantial current densities of ~80 mA/cm$^2$, at an overpotential of 200 mV, and a Tafel slope of 54 mV/decade ($\eta$ = 80-100 mV). From the SEM image (Figure S7) of np-$Mo_2C$ NWs mixed with Vulcan carbon, we can see that the carbon nanoparticles are well-distributed and attached on $Mo_2C$ nanowires allowing the conductive carbon to improve electron transfer between the $Mo_2C$-carbon and the underlying electrode. This was further confirmed by electrochemical impedance measurements. The np-$Mo_2C$ NW/carbon-modified GCE displays lower impedance than an electrode modified with pure np-$Mo_2C$ NWs (Figure 5B). The reduced impedance affords faster electron transfer between the $Mo_2C$ nanocrystallite-carbon mixture and the electrode, contributing to the superior kinetics of the HER. It is anticipated that the catalytic performance will be further improved *via* an *in situ* formation of nanocomposites of $Mo_2C$ on functional carbon based materials.

View Article Online
DOI: 10.1039/C3EE42441C



## Conclusion

In summary, nanoporous $Mo_2C$ nanowires have been successfully demonstrated as highly active and stable catalysts towards the hydrogen evolution reaction. The catalyst was prepared by simply calcining a $MoO_X$/amine hybrid precursor with a sub-nanosized periodic structure. The special features of np-$Mo_2C$ NWs, an enriched nanoporosity by being composed of nanosized crystallites, and a resulting large active surface area, greatly accelerate the interfacial electrochemical reaction and contribute to its potent HER activity. Future perspectives include further augmenting the exceptional catalytic activity of $Mo_2C$ by *in situ* formation of $Mo_2C$ nanocomposites on functional matrices. Such highly catalytic, abundant and inexpensive materials hold great promise for a variety of applications in the fields of energy conversion and storage.

## Experimental

*Reagents*

Ammonium heptamolybdate ($(NH_4)_6Mo_7O_{24}•4H_2O$), aniline, commercial $Mo_2C$, Vulcan carbon and Nafion® perfluorinated ion-exchange resin solution (5% w/w) were purchased from Sigma-Aldrich. Other reagents were obtained from the Shanghai Chemical Plant.

*Synthesis of $Mo_2C$*

The nanoporous molybdenum carbide nanowires (np-$Mo_2C$ NWs) were prepared according to our reported method[22] with modifications. Typically, 2.48 g of ammonium

View Article Online
DOI: 10.1039/C3EE42441C



heptamolybdate and 3.20 g of aniline were added to 40 mL of distilled water and aqueous HCl (1 M) was added drop-wise, with magnetic stirring at room temperature, until a white precipitate was obtained at pH 4~5. After stirring at 50 ℃ for 6 hours, the product was filtered, washed with ethanol and dried at 50 ℃ for a further 10 hours. After expelling air for 4 hours at room temperature using argon, the products obtained above were calcinated at 725 ℃ for 5 hours in an argon flow and, finally, stored in a vacuum desiccator. The molybdenum carbide nanoflake and bulky foam products were prepared by a similar process to that of np-$Mo_2C$ NWs except changing the pH to 1.0 and 2.0, respectively. The morphology of the $Mo_8O_{26}(C_6H_8N)_4 \cdot 2H_2O$ presusor formed at pH 2.0 is bulky and, hence, the bulky foam morphology of the resultant $Mo_2C$ obtained after calcination.[23]

*Characterization*

TEM and SEM images were obtained on JEOL JEM-2011 and Philips XL 30 instruments, respectively. XRD patterns were taken on a Rigaku D/MAX 2000 diffractometer using Cu Kα radiation (λ = 1.54056 Å). $N_2$ sorption isotherms were collected on a Micromeritics ASAP 2010 adsorption analyzer at -196 ℃ (77 K). BET specific surface areas were calculated from adsorption data at a relative pressure range from 0.071 to 0.20. The pore size distribution was derived from the adsorption branch of the isotherms.

*Electrochemical measurements*

The np-$Mo_2C$ NWs (4 mg) were dispersed in 1 mL of solution composed of 4:1 (v/v) distilled water and ethanol containing Nafion (80 μL, 5% wt.) by sonication to form a

View Article Online
DOI: 10.1039/C3EE42441C



homogeneous slurry. Then, 5 μL of the slurry was loaded onto the surface of a home-made glassy carbon electrode (GCE, 3.5 mm in diameter) with a catalyst loading of 0.21 mg/cm$^2$. The np-$Mo_2C$ NW-modified GCE was then dried at room temperature. For comparison, GCEs were also modified with commercial $Mo_2C$, bulky $Mo_2C$, flaky $Mo_2C$ and physical mixtures of np-$Mo_2C$ NW and Vulcan carbon (1:1 w/w). Each modified GCE was loaded with the same amount of catalyst. All electrochemical studies were performed using a CHI660 potentiostat (CH Instruments, China) in a standard three-electrode setup with a modified glassy carbon working electrode, a saturated calomel electrode as a reference, and platinum foil as a counter electrode. The electrocatalytic activity of $Mo_2C$ towards the HER was examined by obtaining polarization curves using linear sweep voltammetry (LSV) at a scan rate of 2 mV/s at room temperature in 0.5 M $H_2SO_4$ solutions. The time dependency of catalytic currents during electrolysis for np-$Mo_2C$ NWs was tested in 0.5 M $H_2SO_4$ at $\eta$ = 130 mV after equilibrium. Electrochemical impedance spectroscopic (EIS) measurements were carried out by an AutoLab in 0.5 M $H_2SO_4$ at different potentials in the frequency range $10^{-2}$ to $10^6$ Hz with a single modulated AC potential of 10 mV. Experimental EIS data were analysed and fitted with the software NOVA 1.7.

**Acknowledgement**

This work was supported by NSFC (20925517), 973 programme (2013CB934101), SKLEAC (201101) and Swiss Science Foundation grant "Solar Fuels" (200 021-134 745). Dr. Heron Vrubel, EPFL Switzerland, is thanked for helpful discussions.

View Article Online
DOI: 10.1039/C3EE42441C





## References

1. J. W. Sun, D. K. Zhong and D. R. Gamelin, *Energy Environ. Sci.* 2010, **3**, 1252-1261.
2. J. O. M. Bockris, *Int. J. Hydrogen Energy*, 2002, **27**, 731-740.
3. N. Armaroli and V. Balzani, *ChemSusChem*, 2011, **4**, 21-36.
4. N. S. Lewis and D. G. Nocera, *Proc. Natl. Acad. Sci. U. S. A.*, 2006, **103**, 15729-15735.
5. M. G. Walter, E. L. Warren, J. R. McKone, S. W. Boettcher, Q. Mi, E. A. Santori and N. S. Lewis, *Chem. Rev.*, 2010, **110**, 6446-6473.
6. D. E. Bartak, B. Kazee, K. Shimazu and T. Kuwana, *Anal. Chem.*, 1986, **58**, 2756-2761.
7. P. Millet, F. Andolfatto and R. Durand, *Int. J. of Hydrogen Energy*, 1996, **21**, 87-93.
8. H. B. Gray, *Nat. Chem.*, 2009, **1**, 7-7.
9. J. L. Dempsey, B. S. Brunschwig, J. R. Winkler and H. B. Gray, *Acc. Chem. Res.*, 2009, **42**, 1995-2004.
10. N. Krstajic, V. Jovic, L. Gajickrstajic, B. Jovic, A. Antozzi and G. Martelli, *Int. J. Hydrogen Energy*, 2008, **33**, 3676-3687.
11. M.-R. Gao, Z.-Y. Lin, T.-T. Zhuang, J. Jiang, Y.-F. Xu, Y.-R. Zheng and S.-H. Yu, *J. Mater. Chem.*, 2012, **22**, 13662.
12. Z. Wu, B. Fang, A. Bonakdarpour, A. Sun, D. P. Wilkinson and D. Wang, *Appl. Catal. B*, 2012, **125**, 59-66.
13. J. D. Benck, Z. Chen, L. Y. Kuritzky, A. J. Forman and T. F. Jaramillo, *ACS Catal.*, 2012, **2**, 1916-1923.
14. S. Wirth, F. Harnisch, M. Weinmann and U. Schröder, *Appl. Catal. B*, 2012, **126**, 225-230.
15. D. V. Esposito, S. T. Hunt, Y. C. Kimmel and J. G. Chen, *J. Am. Chem. Soc.*, 2012, **134**, 3025-3033.
16. C. Ma, J. Sheng, N. Brandon, C. Zhang and G. Li, *Inter. J. Hydrogen Energy*, 2007, **32**, 2824-2829.
17. Y. Wang, S. Song, V. Maragou, P. K. Shen and P. Tsiakaras, *Appl. Catal. B*, 2009, **89**, 223-228.
18. D. Ham, R. Ganesan and J. Lee, *Inter. J. Hydrogen Energy*, 2008, **33**, 6865-6872.
19. M. C. Weidman, D. V. Esposito, Y.-C. Hsu and J. G. Chen, *J. Power Sources*, 2012, **202**, 11-17.
20. H. Vrubel and X. L. Hu, *Angew. Chem. Int. Ed.*, 2012, **51**, 12703-12706.
21. W. F. Chen, C. H. Wang, K. Sasaki, N. Marinkovic, W. Xu, J. T. Muckerman, Y. Zhu and R. R. Adzic, *Energy Environ. Sci.* 2013, **6**, 943-951.
22. Q. Gao, C. Zhang, S. Xie, W. Hua, Y. Zhang, N. Ren, H. Xu and Y. Tang, *Chem. Mater.*, 2009, **21**, 5560-5562.
23. Q. Gao, S. Wang, H. Fang, J. Weng, Y. Zhang, J. Mao and Y. Tang, *J. Mater.*

View Article Online
DOI: 10.1039/C3EE42441C

*Chem.*, 2012, **22**, 4709-4715.

24. J. Kubisztal, A. Budniok and A. Lasia, *Inter. J. Hydrogen Energy*, 2007, **32**, 1211-1218.
25. M. Jafarian, O. Azizi, F. Gobal and M. G. Mahjani, *Int J Hydrogen Energy*, 2007, **32**, 1686-1693.
26. R. K. Shervedani and A. R. Madram, *Electrochim Acta*, 2007, **53**, 426-433.
27. E. Navvaro-Flores and Z. Chong, *J Mol Catal A-Chem.*, 2005, **226**, 179-197.
28. R. Solmaz and G. Kardas, *Inter. J. Hydrogen Energy*, 2011, **36**, 12079-12087.
29. B. E. Conway and B. V. Tilak, *Electrochim. Acta*, 2002, **47**, 3571-3594.
30. J. O. M. Bockris and E. C. Potter, *J. Electrochem. Soc.*, 1952, **99**, 169-186.
31. H. Vrubel, T. Moehl, M. Gratzel and X. Hu, *Chem. Commun.*, 2013, **49**, 8985-8987.

View Article Online
DOI: 10.1039/C3EE42441C



**Figure Captions.**

**Figure 1.** (A) SEM image, (B) TEM image, (C) High-resolution TEM image, (D) EDS pattern, (E) XRD pattern and (F) Nitrogen adsorption/desorption isotherm and pore size distribution (insert) of np-$Mo_2C$ NWs.

**Figure 2.** (A) Polarization curves obtained from glassy carbon electrodes modified with different $Mo_2C$ catalysts, and (B) the corresponding Tafel plots recorded with the catalysts loading of 0.21 mg/cm$^2$; scan rate is 2 mV/s.

**Figure 3.** Nyquist (A) and Bode (B) plots showing EIS responses of a np-$Mo_2C$ NWs-modified glassy carbon electrode at various HER overpotentials in 0.5 M $H_2SO_4$.

**Figure 4.** Stability for the np-$Mo_2C$ NWs-modified electrode with initial LSV polarization curve (---) and after 1000 cycles (—) in 0.5 M $H_2SO_4$ at a scan rate of 10 mV/s. Insert is the time dependence of catalytic currents during electrolysis for np-$Mo_2C$ NWs in 0.5 M $H_2SO_4$ at $\eta$ = 130 mV.

**Figure 5.** (A) Polarization curves of np-$Mo_2C$ NWs and physically mixed with Vulcan carbon (1:1 w/w); scan rate: 2 mV/s. (B) AC impedance spectra of np-$Mo_2C$ NWs and np-$Mo_2C$ NWs/carbon modified GCEs at $\eta$ = 90 mV. The np-$Mo_2C$ NWs/carbon exhibited smaller Faradic impedance.

View Article Online
DOI: 10.1039/C3EE42441C



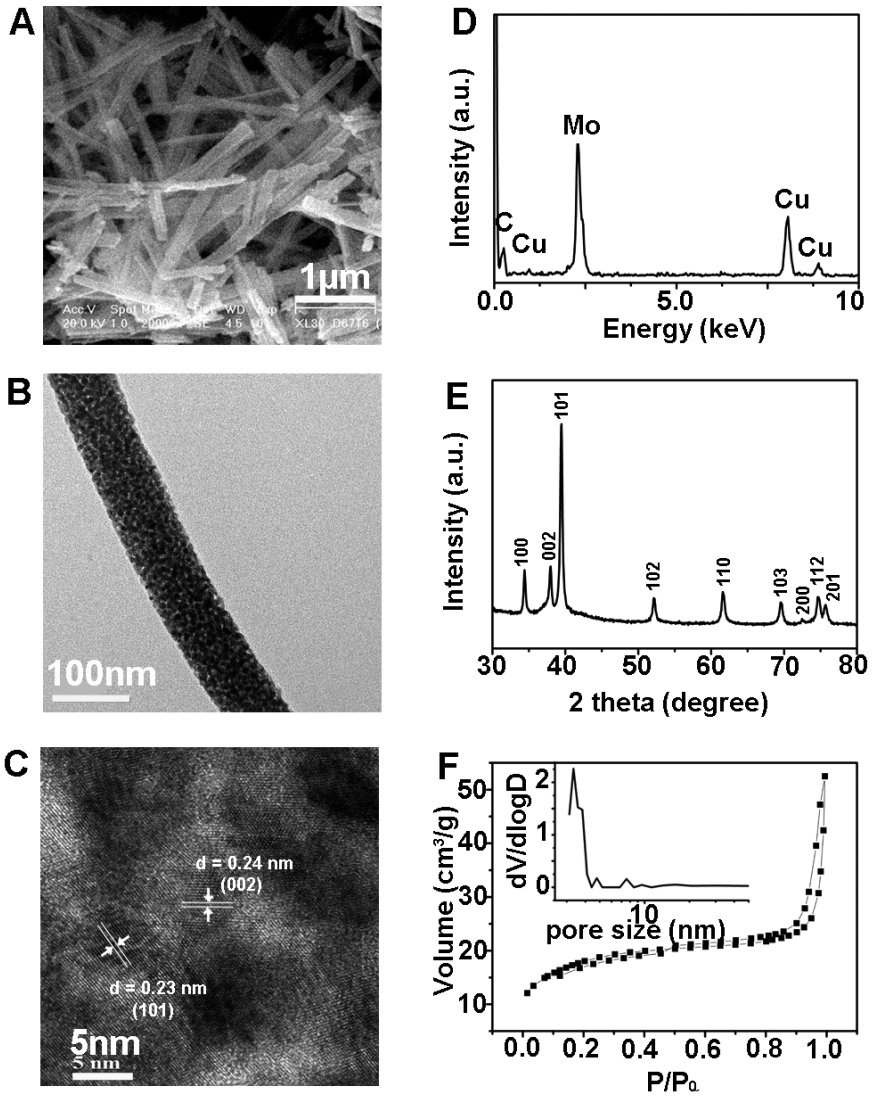


**Figure 1.** (A) SEM image, (B) TEM image, (C) High-resolution TEM image, (D) EDS pattern, (E) XRD pattern and (F) Nitrogen adsorption/desorption isotherm and pore size distribution (insert) of np-$Mo_2C$ NWs.

View Article Online
DOI: 10.1039/C3EE42441C



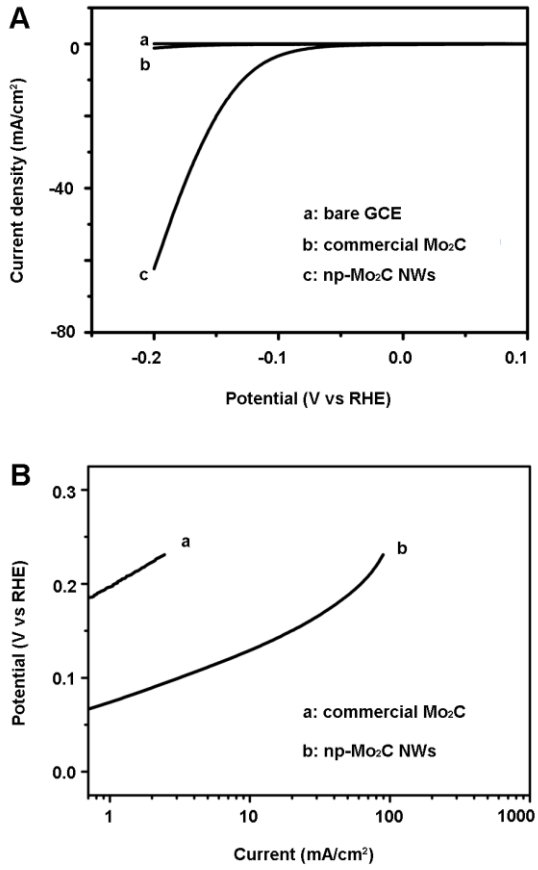


**Figure 2.** (A) Polarization curves obtained from glassy carbon electrodes modified with different $Mo_2C$ catalysts, and (B) the corresponding Tafel plots recorded with the catalysts loading of 0.21 mg/cm$^2$; scan rate is 2 mV/s.

View Article Online
DOI: 10.1039/C3EE42441C



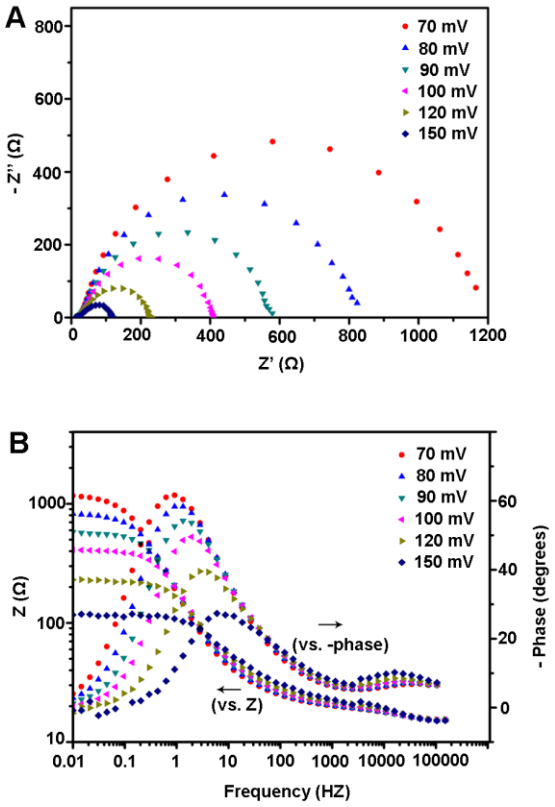


**Figure 3.** Nyquist (A) and Bode (B) plots showing EIS responses of a np-$Mo_2C$ NWs-modified glassy carbon electrode at various HER overpotentials in 0.5 M $H_2SO_4$.

View Article Online
DOI: 10.1039/C3EE42441C



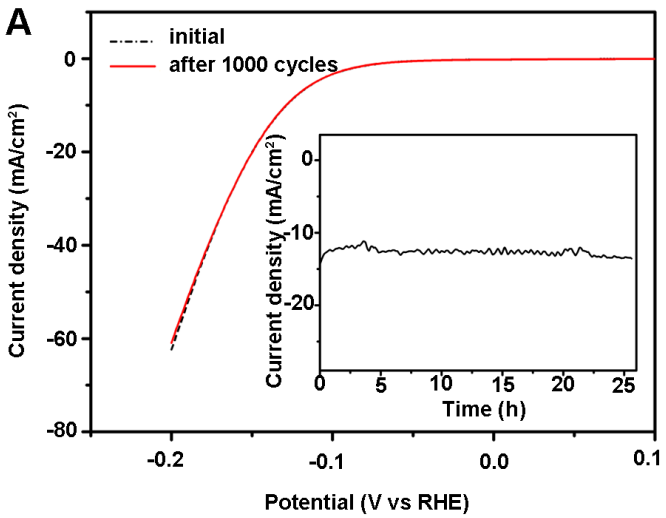


**Figure 4.** Stability for the np-$Mo_2C$ NWs-modified electrode with initial LSV polarization curve (---) and after 1000 cycles (—) in 0.5 M $H_2SO_4$ at a scan rate of 10 mV/s. Insert is the time dependence of catalytic currents during electrolysis for np-$Mo_2C$ NWs in 0.5 M $H_2SO_4$ at $\eta$ = 130 mV.

View Article Online
DOI: 10.1039/C3EE42441C



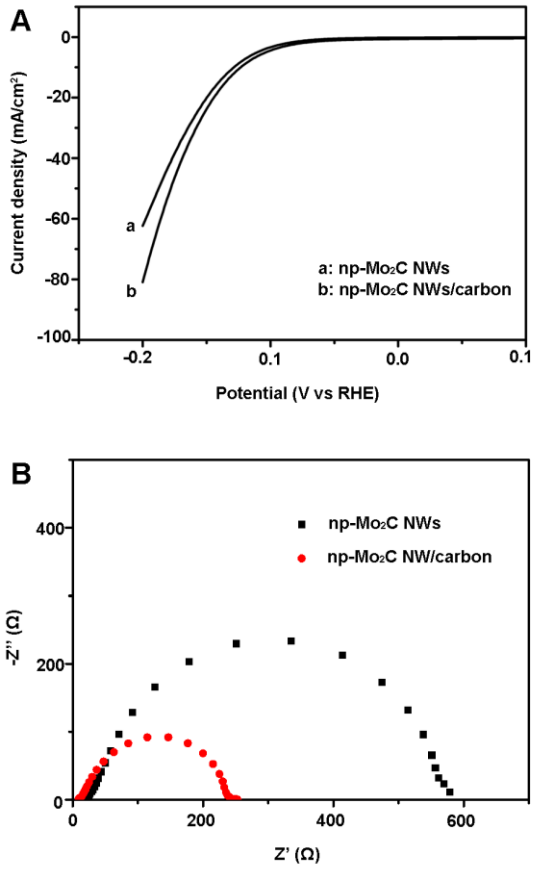


**Figure 5.** (A) Polarization curves of np-$Mo_2C$ NWs and physically mixed with Vulcan carbon (1:1 w/w); scan rate: 2 mV/s. (B) AC impedance spectra of np-$Mo_2C$ NWs and np-$Mo_2C$ NWs/carbon modified GCEs at $\eta$ = 90 mV. The np-$Mo_2C$ NWs/carbon exhibited smaller Faradic impedance.

View Article Online
DOI: 10.1039/C3EE42441C



## Table of Contents

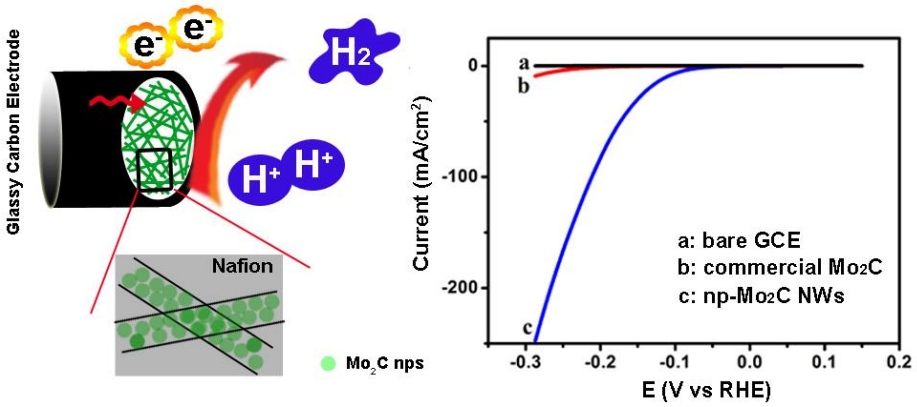


Nanoporous molybdenum carbide nanowires exhibit superior electrocatalytic activity towards the hydrogen evolution reaction due to the abundant nanoporosity, large surface area and high dispersibility of np-$Mo_2C$ NWs.